

Length-scale-dependent phase transition in $\text{Bi}_2\text{Sr}_2\text{CaCu}_2\text{O}_8$ single crystals

K. Vad,* S. Mészáros, and I. Nándori

*Institute of Nuclear Research of the Hungarian Academy of Sciences,
H-4001 Debrecen, P.O.Box 51 Hungary*

B. Sas

*Research Institute of Solid State Physics,
P.O.Box 49, H-1525 Budapest, Hungary*

(Dated: June 28, 2018)

Abstract

Electrical transport measurements using a multiterminal configuration are presented, which prove that in $\text{Bi}_2\text{Sr}_2\text{CaCu}_2\text{O}_8$ single crystals near the transition temperature in zero external magnetic field the secondary voltage is induced by thermally activated vortex loop unbinding. The phase transition between the bound and unbound states of the vortex loops was found to be below the temperature where the phase coherence of the superconducting order parameter extends over the whole volume of the sample. We show experimentally that 3D/2D phase transition in vortex dimensionality is a length-scale-dependent layer decoupling process and takes place simultaneously with the 3D/2D phase transition in superconductivity at the same temperature.

PACS numbers: 74.25.Qt, 74.25.Fy, 74.72.Hs

Keywords:

*Electronic address: vad@atomki.hu

I. INTRODUCTION

Of high- T_c superconducting compounds $\text{Bi}_2\text{Sr}_2\text{CaCu}_2\text{O}_8$ is preferred because its discrete superconducting layers play an important role in current conduction properties even in the transition temperature range. The multicontact configuration is one of the most promising arrangements of electrical transport measurements in the study of superconducting phase transition and vortex dimensionality. In this configuration four electrical contacts are attached to one side of a single crystal and two or four contacts to the opposite side. If the current injected into one side of a crystal is high enough, a voltage drop on both sides can be measured. The side where the current is injected is called primary, the opposite side is secondary. Due to this contact arrangement and the anisotropic conductivity, in $\text{Bi}_2\text{Sr}_2\text{CaCu}_2\text{O}_8$ a non-uniform current distribution develops, and the current injected into the primary side is confined to a very thin surface layer, which is thinner than the thickness of the crystal. If the pancakes in adjacent layers belonging to the same vortex line are strongly coupled to each other, the primary current induces vortex motion both in the primary and in the secondary surface. Moreover, if the coupling strength between the pancakes is high enough to produce three-dimensional (3D) type vortex lines across the sample, primary and secondary voltages can be equal. This configuration is called dc flux transformer configuration.

The first measurements on $\text{Bi}_2\text{Sr}_2\text{CaCu}_2\text{O}_8$ single crystals using the dc flux transformer configuration were performed by Safar *et al.* (1992) and Busch *et al.* (1992). They observed the dimensionality of the vortex system over a wide range of the phase diagram. Wan *et al.* (1993, 1994) and C.D. Keener *et al.* (1997) also used the multicontact dc flux transformer configuration to study the secondary voltage and found that in magnetic fields near the transition temperature the interlayer vortex coupling was responsible for the secondary voltage. However, the origin of the secondary voltage in zero external magnetic field still remained problematic. Pierson (1995) suggested that it originated from thermally activated vortex loop unbinding. A vortex loop is a correlated vortex-antivortex line pair. Using a real-space renormalization group analysis, the author identified three characteristic critical currents and calculated their temperature dependence. He found that the temperature dependence of the secondary voltage is a horizontal slice of the current-temperature phase diagram.

In this paper we present electrical transport measurements using a multiterminal config-

uration that prove the 3D/2D phase transition in vortex dimensionality near the Ginzburg-Landau transition temperature and show that this phase transition is a length-scale-dependent layer decoupling process. We show that the temperature dependence of the secondary voltage in zero magnetic field has a double peak structure.

II. EXPERIMENTAL ARRANGEMENT

Single-crystalline $\text{Bi}_2\text{Sr}_2\text{CaCu}_2\text{O}_8$ compounds were prepared by the melt cooling technique, described in Reference (Cooper *et al.* 1990, Keszei *et al.* 1989). Optically smooth rectangular crystals were carefully cleaved from these compounds, and heated in flowing oxygen for 15 minutes at 900 K in order to stabilize the oxygen content. Chemical homogeneity of the samples was checked by microbeam PIXE and (O^{16}, α) resonant elastic scattering (Rajta *et al.* 1996, Szörényi *et al.* 1998) with a spatial resolution of 5 μm . No chemical inhomogeneities were identified. The surface smoothness was measured by atomic force microscopy. The surfaces were found to be flat with a typical roughness of 10 nm. Before preparing the electrical contacts, the sample quality was checked by magnetization measurements using a SQUID or a vibrating sample magnetometer, and by AC susceptibility measurements. Electrical contacts were made by bonding 25 μm gold wires with Dupont 6838 silver epoxy fired for five minutes at 900 K. The contact resistance was a few ohms. The geometrical position of electrical contacts was precisely measured by optical microscope.

Two current and potential electrodes were attached to both faces of the crystals. The scheme of the electrode configuration is shown in Fig. 1. The current was injected into one face of the single crystal through the current contacts (this is the primary current I_P), while primary and secondary longitudinal voltages, and the voltage between the two faces were recorded simultaneously.

We have performed measurements on a few crystals fabricated from the same batch. The mean-field Ginzburg-Landau (GL) transition temperature T_{c0} of the samples was 88 K. The sample dimensions were about $1 \times 1.5 \text{ mm}^2$, the thickness was between 8 and 3 μm . As we pointed out in our previous papers (Portier *et al.* 2000, Sas *et al.* 2000), most of the Joule heat due to the transport current was generated in the current contacts. In order to reduce the heat dissipation, and also to eliminate the thermoelectric force, we used current pulses with a duration time of 1 ms and repetition time of 100 ms. This arrangement

and the fact that the sample temperature was regulated by a temperature controlled He gas stream instead of exchange gas, made it possible to avoid heating during the pulse up to the amplitude of 10 mA. Using the analysis of Busch *et al.* (1992), we could define the temperature dependence of the ab plane and c -axis resistivities from the voltages V_{PL} and V_{SL} . For the anisotropy ratio γ we received $\gamma = \sqrt{(\rho_c/\rho_{ab})} \approx 500$ with $\rho_{ab} \approx 100 \mu\Omega\text{cm}$ at 90 K.

III. MEASUREMENTS

In our experiments the following voltages, shown in Fig. 1, were simultaneously recorded: (i) longitudinal voltages measured parallel to the current direction on the surface of the crystal where the current was injected and on the opposite surface, i.e., primary and secondary longitudinal voltages (V_{PL} and V_{SL}); (ii) the c -axis direction voltage measured between the two surfaces of the crystal (V_C).

The temperature dependence of the primary and secondary longitudinal voltages of a $\text{Bi}_2\text{Sr}_2\text{CaCu}_2\text{O}_8$ single crystal measured in zero magnetic field is shown in Fig. 2. In zero applied magnetic field the secondary voltage is determined by interlayer vortex coupling. In order to gain information about this coupling strength, we measured the voltage V_C between the two surfaces of the crystal while applying a primary current I_P . Depending on the current distribution in the crystal, some part of this current flows in the c -axis direction and V_C depends on this current. The temperature dependence of V_C is of metallic ($d\rho/dT > 0$) type, except in a small temperature range near the mean-field Ginzburg-Landau transition temperature. In Fig. 3(a) this range is between 85 and 86 K. This temperature dependence is also reflected in the current-voltage characteristics (Fig. 3(b)). Far above the GL transition temperature, at 256 K the current-voltage characteristic is linear. Near the GL transition temperature, at 87.3 K there is a slight curvature in it. On further cooling the sample from 87.3 K to 86 K the curvature increases. In the temperature range between 86 K and 85 K the $I_P - V_C$ curves are concave in shape (for clarity in Fig. 3 we present only the curve measured at 85.8 K). At temperatures lower than 85 K both the $V_C - I_P$ and $V_C - T$ curves show the same metallic behavior, as above 86 K.

IV. RESULTS AND DISCUSSION

In 2D superconducting layers the phase fluctuation of the order parameter generates vortex-antivortex pairs as topological excitations (Tinkham 1996). The phase transition in an isolated 2D superconducting layer, where the vortex-antivortex pairs are bound below the phase transition temperature and are unbound above it, is described by the Kosterlitz-Thouless theory (Halperin and Nelson 1979, Kosterlitz and Thouless 1973). In thin films, if the film thickness is less than the superconducting coherence length, this Kosterlitz-Thouless phase transition (T_{KT}) can be observed.

In high-temperature superconductors, the high transition temperature, short coherence length and layered structure make the phase fluctuation of the order parameter dominant over the other fluctuations in the transition temperature range, but the coupling between superconducting layers modifies the 2D Kosterlitz-Thouless picture. The interaction between superconducting layers leads to vortex-antivortex interaction different from the 2D case. In $\text{Bi}_2\text{Sr}_2\text{CaCu}_2\text{O}_8$ single crystals the CuO_2 planes serve as 2D superconductor layers, the vortices are the pancake vortices. Due to the layered structure a high anisotropy exists in conductivity and the vortex matter has a very rich phase diagram with numerous phase transitions. Among others the 3D phase appears, where the coupling between neighboring layers arranges the thermally excited pancake vortices into 3D flux lines (Blatter *et al.* 1994). These 3D flux lines can form vortex loops as correlated vortex-antivortex line pairs. They are called thermally activated vortex loops, because they are the result of a combined effect of thermally activated vortex excitation and interlayer vortex coupling.

The 3D character modifies the structure of the phase transition between the bound and unbound states: a narrow 3D window appears around the phase transition temperature (T_c) and a nonzero critical current appears. The 3D temperature region is theoretically predicted and it has been shown that the size of this 3D region is much smaller above T_c than below (Pierson 1995). Above the phase transition temperature the behavior of vortices becomes 2D due to decoupling of the superconducting layers (3D/2D phase transition). This layer decoupling is a length-scale-dependent process: the layers become decoupled at length scales larger than an interlayer screening length, while for lengths below this scale they remain coupled.

In an isolated 2D superconducting layer the vortex pair energy is the sum of the creation

energy of the two vortices and the intralayer logarithmic coupling energy between vortices. In layered systems like $\text{Bi}_2\text{Sr}_2\text{CaCu}_2\text{O}_8$ this vortex pair energy is modified by the interlayer Josephson coupling, which not only strengthens the intralayer interaction, but causes an interaction between vortices located in neighboring layers. The intralayer vortex pair energy can be written in the following simple form: $E(r) = 2E_c + K_{\parallel}\ln(r/\xi_0) + K_{\perp}r/\xi_0$, where r is the distance between the vortex and antivortex, E_c is the creation energy of a vortex, ξ_0 is the zero-temperature correlation length, K_{\parallel} is the intralayer vortex-vortex coupling constant and K_{\perp} is the interlayer Josephson coupling constant. While the 2D logarithmic interaction (second term in this equation) dominates at short distances, the Josephson-coupling mediated 3D linear interaction (third term) dominates at large distances. The intralayer vortex length scale $R_{\lambda}(T)$ is the characteristic length which divides this logarithmic and linear regimes (Pierson 1995-II). $R_{\lambda}(T) = \xi_0/\sqrt{\lambda}$, where λ is the ratio of the interlayer Josephson coupling to the intralayer coupling, $\lambda = K_{\perp}/K_{\parallel}$. λ depends on the size r of the vortex pairs, and above T_c it has a maximum. The size r which belongs to this maximum λ is the other characteristic length, the interlayer screening length $l_{3D/2D}(T)$. If the separation between two vortices located in neighboring layers is larger than $l_{3D/2D}$, the Josephson-coupling mediated linear interaction is screened out and the layers are decoupled. Around T_c the dimensional behavior of the system is determined by these two characteristic lengths. The layers are coupled and the behavior of vortices is 3D if the separation between vortices is greater than the intralayer vortex length scale $r > R_{\lambda}(T)$ and less than the interlayer screening length $r < l_{3D/2D}(T)$. The temperature dependence of $R_{\lambda}(T)$ and $l_{3D/2D}(T)$ shows (Pierson 1995-III) that the intralayer vortex length scale $R_{\lambda}(T)$ is constant for $T \ll T_c$, but it increases as the temperature approaches T_c from below. The interlayer screening length $l_{3D/2D}(T)$ decreases continuously as the temperature increases.

While in the 3D regime below T_c the electrical transport behavior is dominated by vortex loops, above T_c it is dominated by vortex lines and pancake vortices. The multiterminal configuration is a good arrangement to distinguish between these two regimes, and the temperature dependence of the secondary voltage can help us to understand the length-scale-dependent layer decoupling, i.e., the 3D/2D phase transition.

The secondary voltage has already been studied both theoretically (Pierson 1995) and experimentally (Wan *et al.* 1993). It can now be accepted that in zero applied magnetic field it originates from thermally activated vortex loop unbinding. At low temperatures

where V_{SL} and V_{PL} are zero, the thermally excited 3D flux lines form vortex loops which are 'pinned' to the crystal. With increasing temperature, the transport current splits these vortex loops into free vortex-antivortex line pairs. The temperature where this splitting starts is the unbinding temperature (T_{UB}). This is the lowest temperature where both V_{SL} and V_{PL} are observable. Above the unbinding temperature the free vortices move in the sample like 3D vortex lines due to the Lorentz force, producing the same voltage drop on the primary and secondary side of the crystal, $V_{PL} = V_{SL}$. This 3D character of the vortex lines remains up to a temperature where the secondary voltage has a local maximum. In Fig. 2 the 3D temperature range is around 85 K where the primary and secondary longitudinal voltages V_{PL} and V_{SL} coincide. This is the same 3D temperature range which was predicted theoretically by renormalization group analysis (Pierson 1995). With increasing temperature the 3D character of flux motion disappears and consequently V_{SL} becomes lower than V_{PL} , but another local maximum of V_{SL} can be found as the temperature approaches T_{c0} . The temperature dependence of the secondary voltage has two peaks with a higher and a lower amplitude.

This double peak structure of V_{SL} can be explained by the motion of different types of vortex lines. In zero applied magnetic field free vortex lines can be produced in two ways. First, they can be the result of vortex-antivortex depairing of thermally activated vortex loops due to the Lorentz force of the transport current. In this case the number of free vortex lines depends on the transport current density and a non-Ohmic behavior characterizes the system. Secondly, free vortex lines can be spontaneously created by thermal activation, mainly above T_c . The number of free vortex lines increases with increasing temperature and the system is characterized by an Ohmic behaviour. In Fig. 4 we illustrate the different types of vortices and vortex dimensionalities schematically.

The effect of current on vortex-antivortex depairing is twofold. On the one hand the current reduces the creation energy whereby increases the density of vortex pairs. On the other hand the current exerts a force (the Lorentz force) on vortex loops and can blow them out. The number of blowouts depends on the size r of the vortex pairs. If r is higher than the intralayer vortex length scale $R_\lambda(T)$, the Josephson-coupling mediated 3D linear interaction is energetically favored over 2D intralayer logarithmic interaction and the energy of a vortex loop is smaller than the energy of a pair of independent vortex lines. Below T_c in $\text{Bi}_2\text{Sr}_2\text{CaCu}_2\text{O}_8$ $R_\lambda(T) = \xi_0/\sqrt{\lambda} \approx 1\mu\text{m}$, where $\xi_0 \sim 3\text{nm}$ and $\lambda \sim 10^{-5}$. Consequently, if

$r > 1\mu\text{m}$, creation of vortex loops is energetically favored over free vortex-antivortex line pairs. This happens in the 3D temperature range where the dominant topological excitation is the vortex loop. With increasing temperature the number of blowouts and, so, the secondary voltage increases. However, approaching the transition temperature the intralayer vortex length scale $R_\lambda(T)$ starts to increase, therefore the number of vortex pairs which can be blown out by the transport current decreases which results in the decrease of the secondary voltage. The temperature which belongs to the peak value of the secondary voltage is the transition temperature T_c . Although at this temperature the behavior of vortices is still 3D type as it was shown theoretically (Pierson 1995-III), the secondary voltage is somewhat lower than the primary voltage (see Fig. 2). This means that the secondary voltage starts to decrease before layer decoupling. At higher temperatures the 3D character of flux motion disappears and V_{SL} becomes significantly lower than V_{PL} . Above the 3D temperature range another local maximum of V_{SL} can be found as the temperature approaches T_{c0} , because the temperature is high enough to produce free vortex lines by thermal activation. The number of free vortex lines and, so, the secondary voltage increases with increasing temperature. The system is characterized by a continuous 3D/2D transition due to continuous decrease of the interlayer screening length $l_{3D/2D}(T)$ as the temperature approaches the mean-field Ginzburg-Landau transition temperature T_{c0} . Near T_{c0} the amplitude of the order parameter decreases, just as the number of the free vortex lines. This effect evokes the decrease of the secondary voltage. The temperature which belongs to the minimum secondary voltage above the double peak structure is T_{c0} .

Information about the strength of Josephson coupling and the 2D/3D phase transition in superconductivity can be obtained by study the temperature dependence of $I_P - V_C$. In the temperature range where the $I_P - V_C$ curves are concave (between 85 and 86 K) the superconducting coherent state exists in the CuO_2 bilayers, but the interlayer coupling is not strong enough to establish the c -axis coherence. In consequence, the current in c -axis direction is carried by single particle tunnelling instead of Cooper pair tunnelling (2D type superconductivity). There is no stabil phase coherence between superconducting bilayers and the phase fluctuation is dominant. Consequently, the shape of the $V_C - T$ curve in the temperature range where $d\rho/dT < 0$ can slightly change at different sample cooling rates. Figure 3 presents the $V_C - T$ and $V_C - I_P$ curves taken at different sample cooling rates. With the decrease in temperature, at 85 K, the Josephson coupling, and consequently, a phase

coherence between superconducting bilayers develops and extends over the whole volume of the sample, producing maximum values in both V_{SL} and V_C (2D/3D phase transition). At temperatures lower than 85 K the Josephson coupling energy increases, the phase coherence of the superconducting order parameter extends over the whole volume of the sample and develops the 3D type superconductivity. The higher peak value of V_{SL} is also at 85 K which is the upper end of the temperature range where vortex lines have 3D character. Consequently 2D/3D phase transition in superconductivity and in vortex dimensionality takes place at the same temperature. This can be valid inversely, too. If the vortex dimensionality decreases from 3D to 2D, the dimensionality of superconductivity can also decrease. This result was experimentally supported by transport current measurements (Pethes *et al.* 2001), where the authors proved that the Bardeen-Stephen model for the flux flow resistance $\rho_f = \rho_n \cdot B/B_{c2}$ (ρ_n , B and B_{c2} are the normal state resistivity, magnetic field and critical magnetic field) is not valid at high current density in $\text{Bi}_2\text{Sr}_2\text{CaCu}_2\text{O}_8$ single crystals. Due to intensive flux motion both the phase coherence between superconducting bilayers and the interlayer screening length $l_{3D/2D}(T)$ decrease resulting in a 3D/2D phase transition in dimensionality of superconductivity.

V. CONCLUSIONS

In conclusions, we found that temperature dependence of secondary longitudinal voltage has a double-peak structure and its higher maximum value is at the temperature where the phase coherence of the order parameter extends over the whole sample. Secondary voltage originates from correlated vortex-antivortex line pair unbinding, i.e., from vortex loop unbinding due to the Lorentz force of the transport current. Near T_{c0} free vortex-antivortex line pairs are also generated by thermally activated vortex excitation. We think that the two types of vortex-antivortex line pairs are responsible for the double peak structure of the secondary longitudinal voltage. Lacking of theories describing this double peak structure in $\text{Bi}_2\text{Sr}_2\text{CaCu}_2\text{O}_8$ single crystals indicates a need for better description of length-scale dependence in layered superconductors. In order to improve the theoretical description, one can perform the renormalization group analysis of Reference (Pierson 1995) for non-constant current density or one can use different renormalization group methods, e.g., field theoretical renormalization group approaches (Nandori *et al.* 2004, 2001).

Acknowledgments

We take great pleasure in acknowledging discussion with P.F. de Châtel. This work was supported by the Hungarian Science Foundation (OTKA) under contract no. T037976.

BLATTER G., FIEGEL'MAN M.V., GESHKENBEIN V.B., LARKIN A.I. and VINOKUR V.M., 1994, *Reviews of Modern Physics* **66**, 1125.

BUSCH R., RIES G., WERTHNER H., KREISELMEYER G. and SAEMANN-ISCHEENKO G., 1992, *Phys. Rev. Lett.* **69**, 522.

COOPER J. R., FORRÓ L. and KESZEI B., 1990, *Nature* **343**, 444.

HALPERIN B.I. and NELSON D.R., 1979, *J. Low Temp. Phys.* **36**, 599.

KEENER C. D., TRAWICK M. L., AMMIRATA S. M., HEBBOUL S. E. and GARLAND J. C., 1997, *Phys. Rev. B* **55**, R708.; 1997, *Phys. Rev. Lett.* **78**, 1118.

KESZEI B., SZABÓ Gy., VANDLIK J., POGÁNY L. and OSZLÁNYI G., 1989, *J. Less Common Metals* **155**, 229.

KOSTERLITZ J.M. and THOULESS D.J., 1973, *J. Phys. C* **6**, 1181.

NÁNDORI I., JENTSCHURA U.D., SAILER K. and SOFF G., 2004, *Phys. Rev. D* **69**, 025004.; and 2002, *J. Phys. G* **28**, 607.;

NÁNDORI I., POLONYI J. and SAILER K., 2001, *Phil. Mag. B* **81**, 1655.; and 2001, *Phys. Rev. D* **63**, 045022.

PETHES I., SAS B., KRIZA G., PORTIER F., WILLAMS F.I.B., VAD K. and MÉSZÁROS S., 2001, *Synthetic Metals* **120**, 1013.

PIERSON S. W., 1995, *Phys. Rev. Lett.* **74**, 2359.; 1997, *Phys. Rev. B* **55**, 14536.

PIERSON S.W., 1995, *Phys. Rev. B* **51**, 6663.

PIERSON S.W., 1995, *Phys. Rev. Lett.* **75**, 4674.

PIERSON S.W., 1995, *Phys. Rev. B* **54**, 688.

PIERSON S.W., 1992, *Phys. Rev. B* **45**, 13035.

PORTIER F., KRIZA G., SAS B., KISS L.F., PETHES I., VAD K., KESZEI B., WILLAMS N. and F.I.B., 2002, *Phys. Rev. B* **66**, 140511(R).

RAJTA I., BORBÉLY-KISS I., MÓRIK GY., BARTHA L., KOLTAY E. and KISS Á. Z., 1996, *Nucl. Inst. and Methods B* **109**, 148.

SAFAR H., RODRIGUEZ E., de la CRUZ F., GAMMEL P. L., SCHNEEMEYER L. F. and BISHOP D. J., 1992, *Phys. Rev. B* **46**, 14238.

SAS B., PORTIER F., VAD K., KESZEI B., KISS L. F., HEGMANN N., PUHA I., MÉSZÁROS

S. and WILLAMS F. I. B., 2000, *Phys. Rev. B* **61**, 9118.

SZÖRÉNYI T., GERETOVSZKY Zs., KELEMEN L., TÓTH J. and SIMON A., 1998, *Vacuum* **59**, 327.

TINKHAM M., 1996, *Introduction to Superconductivity* (McGraw-Hill, New York).

WAN Y. M., HEBBOUL S. E., HARRIS D. C. and GARLAND J. C., 1993, *Phys. Rev. Lett.* **71**, 157.

WAN Y. M., HEBBOUL S. E. and GARLAND J. C., 1994, *Phys. Rev. Lett.* **72**, 3867.

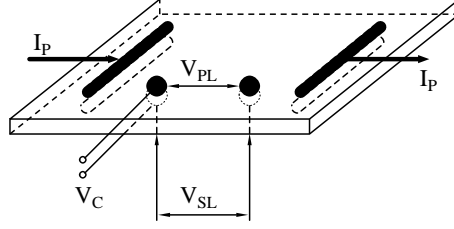


FIG. 1: Electrode configuration used for secondary voltage measurements. V_{PL} and V_{SL} denote the primary and secondary longitudinal voltages, V_C and I_P denote the c -axis direction voltage and the primary current, respectively.

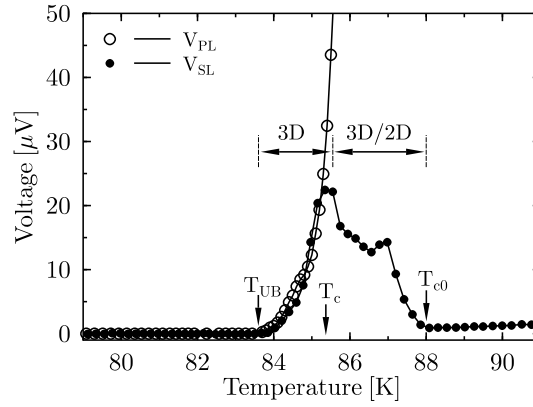


FIG. 2: Secondary and primary voltages vs. temperature in zero magnetic field, $I_P = 1$ mA. T_{UB} , T_c and T_{c0} denote the unbinding, transition and Ginzburg-Landau transition temperature, respectively. The different vortex dimensionalities are also shown.

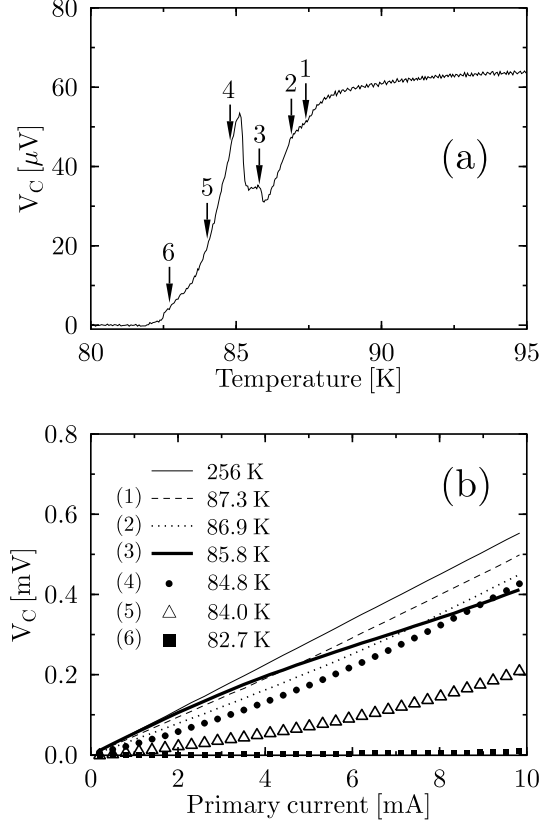


FIG. 3: Temperature dependence of V_C at 1 mA primary current (a), and current-voltage characteristics measured at different temperatures (b) in zero magnetic field. The arrows in (a) denote the temperatures where the current-voltage characteristics were measured.

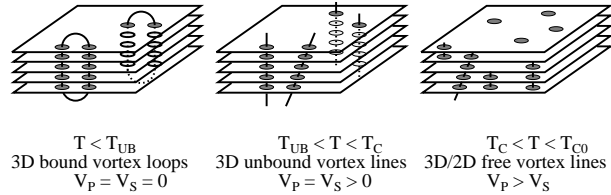


FIG. 4: Schematic illustration of different vortex types.